Desalination and Water Treatment
www.deswater.com
doi: 10.1080/19443994.2015.1067168

57 (2016) 7801–7811
April

Taylor & Francis
Taylor & Francis Group

Functionalization of zinc oxide (ZnO) nanoparticles and its effects on polysulfone-ZnO membranes

Ying Tao Chung[a], Muneer M. Ba-Abbad[a,b], Abdul Wahab Mohammad[a,b,*], Abdelbaki Benamor[c]

[a]*Faculty of Engineering and Built Environment, Department of Chemical and Process Engineering, Universiti Kebangsaan Malaysia, UKM Bangi, Selangor 43600, Malaysia, emails: cytao518@gmail.com (Y.T. Chung), muneer711@gmail.com (M.M. Ba-Abbad), wahabm@eng.ukm.my (A.W. Mohammad)*
[b]*Faculty of Engineering and Built Environment, Research Centre for Sustainable Process Technology (CESPRO), Universiti Kebangsaan Malaysia, Bangi, Selangor 43600, Malaysia,*
[c]*Gas Processing Center, Qatar University, Doha, Qatar, email: benamor.abdelbaki@qu.edu.qa*

Received 31 January 2015; Accepted 19 June 2015

ABSTRACT

Incorporation of nanoparticles in membranes has recently been reported to lead to enhancement of the membrane performance for various applications. In this study, ZnO nanoparticles were synthesized via sol–gel method using zinc acetate and oxalic acid as starting materials. However, the influence of additive, in this case ethylene glycol (EG), on the size of ZnO nanoparticles produced was investigated. All diffraction peaks of XRD patterns indicated the wurtzite structure and the hexagonal phase of ZnO nanoparticles. Uniform spherical particle sizes with lower sizes and reduced agglomeration were observed when EG was used under the same experimental conditions. The particle size was found in the range of 20–30 nm when EG was used as compared to those without EG, which was between 50–60 nm. Dispersion property of the ZnO NPs was further verified by zetasizer analysis. Subsequent incorporation of the smaller size ZnO nanoparticles in membranes has shown improvement in the characteristics and performance of the membranes. Membranes incorporated with ZnO showed improved hydrophilicity and enhancement of membrane performance in terms of permeability, porosity, and rejection ability.

Keywords: Zinc oxide; Nanoparticles; Functionalization; Additives

1. Introduction

Recent reports showed that the use of nanoparticles (NPs) is increasing in various industrial applications such as medical, biomedical, pharmacy, etc. This was mainly due to the outstanding characteristics of NPs which attract great attention. NPs can be defined as particles or crystallites with nanoscale dimensions. The reduced size of NPs may lead to higher efficiency due to the availability of higher surface area. When the particles have been produced in such small sizes,

*Corresponding author.

Presented at the 7th International Conference on Challenges in Environmental Science and Engineering (CESE 2014) 12–16 October 2014, Johor Bahru, Malaysia

their reactivity changed significantly. For example, metallic NPs can easily donate their electrons to the surrounding compounds to form radicals by reducing agents or when these NPs are exposed to the external energy source such as UV light. The excellent physical and chemical properties of NPs could be summarized in terms of catalytic, antibacterial, mechanical, electronic, optical, magnetic, etc. [1]. Several kinds of NPs have been widely applied such as titanium dioxide (TiO_2), silicon dioxide (SiO_2), silver (Ag), polyaniline (PANI), zinc oxide (ZnO), and so forth [2].

The use of NPs in development of membranes has been increasing recently. A number of studies have reported on the incorporation of NPs in membranes and subsequent applications, for example, in water and wastewater treatment [3–5]. All these studies reported the significant enhancement membrane performance in terms of antifouling and antibacterial properties [6,7]. Recent work has reported on the membrane modification using ZnO NPs. Due to its special properties, ZnO NPs has great ability to increase membrane permeability, mechanical properties, hydrophilicity, fouling resistance, and selectivity [8]. Blending zinc oxide (ZnO) NPs into PSF membranes has been reported to improve the membrane properties in reducing fouling by oleic acid, improved thermal stability, and permeability [9].

Functionalization of NPs has been reported to be able to enhance the NPs effectiveness. Functionalization could be defined as surface coating or capping which assists in regulating the properties of NPs in terms of stability, solubility, and targeting characteristics. The synthesis process parameters play an important role in producing fine quality of NPs. For instance, the molar ratio, pH of reactants, and capping agents will affect the size of ZnO NPs [10]. Besides, the doping activity onto the NPs would give impacts on the properties of NPs [11]. The effect of solvents on the synthesis of nanosize zinc oxide and its properties were also investigated [12]. The polymer adsorption such as polyvinyl alcohol and polyethylene glycol by NPs also improved the stability of NPs against agglomerations [13].

Hence, the main objective of this study is to investigate the influence of additive Ethylene glycol (EG) towards the size of ZnO NPs. The purpose of functionalization is to enhance the size reduction of particles and also overcoming agglomerations problems. The properties of synthesized ZnO NPs would be characterized by several techniques such as Thermogravimetry-Differential Scanning Calorimetry (TGA-DSC), X-ray diffraction (XRD), Transmission Electron Microscopy (TEM), Field Emission Scanning Electron Microscopy (FESEM), and Fourier Transform Infrared Spectroscopy (FTIR). Finally, the synthesized ZnO NPs with functionalization was applied in membrane fabrication and the performance of the membrane was investigated.

2. Experimental

2.1. Materials

Zinc acetate dehydrate [$Zn(CH_3COO)_2{\cdot}2H_2O$], oxalic acid dehydrate [$H_2C_2O_4{\cdot}2H_2O$], absolute ethanol (99%), and EG were analytical grade and purchased from Merck. All chemicals were used for the synthesis process without any further purification.

2.2. Synthesis of ZnO NPs

ZnO NPs were synthesized via sol–gel method using zinc acetate dehydrate and oxalic acid dehydrate as starting materials [14]. Zinc acetate and oxalic acid mixtures (Zac/Oxa) were prepared in ethanol with molar concentrations ratio of 0.1:0.15 at Zac/Oxa ratio of 40/60. The zinc acetate and oxalic acid were dissolved in ethanol at 60 ± 5 and 50 ± 5°C, respectively, under reflux condition for 30 min. Meanwhile, EG which acted as surfactant was added into zinc acetate solution after 30 min of heating. The oxalic acid solution was then added dropwise to the zinc acetate solution. The mixture was then left under vigorous magnetic stirring for 90 min to allow the complete reaction in obtaining a gel-like zinc oxalate. The operating pH of 2.0 ± 0.2 was obtained by initial addition of oxalic acid to the mixture [10]. The resulting gel was dried at 60°C overnight in the oven to form the precursors for the ZnO NPs and the ZnO NPs were then taken to undergo calcination at temperature of 400°C for 3 h.

2.3. Characterizations of ZnO NPs

2.3.1. Thermogravimetry-differential scanning calorimetry

The thermal-decomposition behavior of the zinc oxalate precursor was analyzed using TGA-DSC (STA 449F3, Jupiter, Netzsch, Germany). The temperature was increased from 30 to 800°C at a heating rate of 10°C/min.

2.3.2. X-ray diffraction

The crystal phase composition and the crystallite size of the ZnO NPs could be determined using XRD (Bruker D8 Advance AXS X-ray diffractometer) with

CuKα radiation (1.5406 Å) in the 2 h scan range of 20–80˚.

The average crystallite size of the ZnO was further determined from the XRD patterns using the Debye–Scherer equation (Eq. (1)).

$$D = K\lambda/\beta\cos\theta \quad (1)$$

where K is the Scherer constant ($K = 0.89$), k is the X-ray wavelength, b is the peak width at half maximum, and h is the Bragg diffraction angle.

2.3.3. Fourier transform infrared spectroscopy

The FTIR spectra of the ZnO NPs were recorded using the Thermo/Scientific, NICOLET 6700.

2.3.4. Transmission electron microscopy

The size of the ZnO NPs was investigated using a transmission electron microscope (Philips CM200, model JEOLJEM 2100).

2.3.5. Field emission scanning electron microscopy

The morphology and structure of the NPs were investigated using high-resolution FESEM (SUPRA 55VP) with energy dispersive X-ray spectroscopy (EDX) (Oxford EDX INCA Penta FETX3).

2.3.6. Zetasizer Analysis

The dispersion property of ZnO NPs were measured using the Zeta Sizer, model Nano-ZS, Malvern instruments Inc. (UK). The dispersion of ZnO NPs was checked by applying 0.1% w/v (weight of ZnO/volume of water as solvent) under 30 min of sonication before the analysis. This is to ensure the equal distribution of ZnO NPs in the solution.

2.4. Membrane application

2.4.1. Membrane fabrication

The synthesized ZnO NPs were applied in membrane fabrication via wet phase inversion technique. ZnO NPs were incorporated during the preparation of polysulfone (PSF) casting solution. The casting solution was prepared by dissolving 16% of PSF pellets into 1-methyl-2-pyrrolidinone (NMP) in a water bath with average temperature of 75˚C under continuous stirring condition for about 5 h. ZnO NPs were sonicated for better dispersion before mixing in the homogeneous PSF casting solution. The membranes were casted using Filmographe Doctor Blade 360099003 (Braive Instrument, Germany) with thickness of 0.2 mm. The fabricated membranes were then kept with UP water for storage.

2.4.2. Membrane characterization

2.4.2.1. Membrane permeability. The permeability of membrane was determined by measuring the pure water fluxes using a stirred cell (Sterlitech HP4750). The pure water flux was calculated using the following equation:

$$J = V/S\ t \quad (2)$$

where J is the water flux (L m^{-2} h^{-1}); V is the permeate volume (L); S is the effective membrane area (m^2); t is the operation time (h^{-1}). Graph of water fluxes against pressures was plotted and the permeability was determined based on the gradient of the linear line.

2.4.2.2. Surface hydrophilicity study. The angle between water and membrane surface was measured with contact angle meter, Model Kruss GmbH, Germany with Drop Shape Analysis software. Based on the differences of the contact angle values for each membrane, the membrane surface hydrophilicity was compared.

2.4.2.3. Membrane porosity. The overall porosity (ε) was determined using gravimetric method, as defined in the following equation:

$$\varepsilon = \frac{\omega_1 - \omega_2}{A \times t \times d_w} \quad (3)$$

where ω_1 is the wet membrane weight, ω_2 is the dried membrane weight, A(m^2) is the area of the membrane, t is the thickness, and d_w is the water density (998 kg/m^3). The pore size of membranes was calculated using the porosity data and Guerout–Elford–Ferry equation (Eq. (4)).

$$r_m = \sqrt{\frac{(2.9 - 1.75\varepsilon)8\eta l Q}{\varepsilon \times A \times \Delta P}} \quad (4)$$

where η is the water viscosity (8.9×10^{-4} Pa s), Q is the volume of permeated pure water per unit time (m^3/s), and ΔP is the operational pressure (MPa).

2.4.2.4. Morphological study. The surfaces and cross-sectional structures of the unmodified and modified membranes were obtained using scanning electron microscope (SEM, Gemini SUPRA 55VP-ZEISS).

2.4.2.5. Rejection study. Humic acid solution of 10 ppm was used to test the rejection of membranes. The permeate fluxes and rejections of humic acid can thus be determined. The rejection was determined using the following equation:

$$R = 1 - C_p/C_f \quad (5)$$

where C_p is the permeate solution concentration and C_f is the feed solution concentration.

3. Results and discussion

3.1. Thermogravimetry analysis of ZnO NPs (TGA-DSC)

The thermal characteristics of ZnO and ZnO-EG precursors were investigated by applying TGA and the DSC methods. Fig. 1 exhibits the heating profile and weight losses of ZnO and ZnO-EG throughout the calcination process. Generally, the weight loss shown in TGA-DSC spectrum was attributed to the reactions between zinc acetate and oxalic acid. The equations below stated several decomposition stages of the starting materials in different temperature range in order to obtain the final product of pure ZnO.

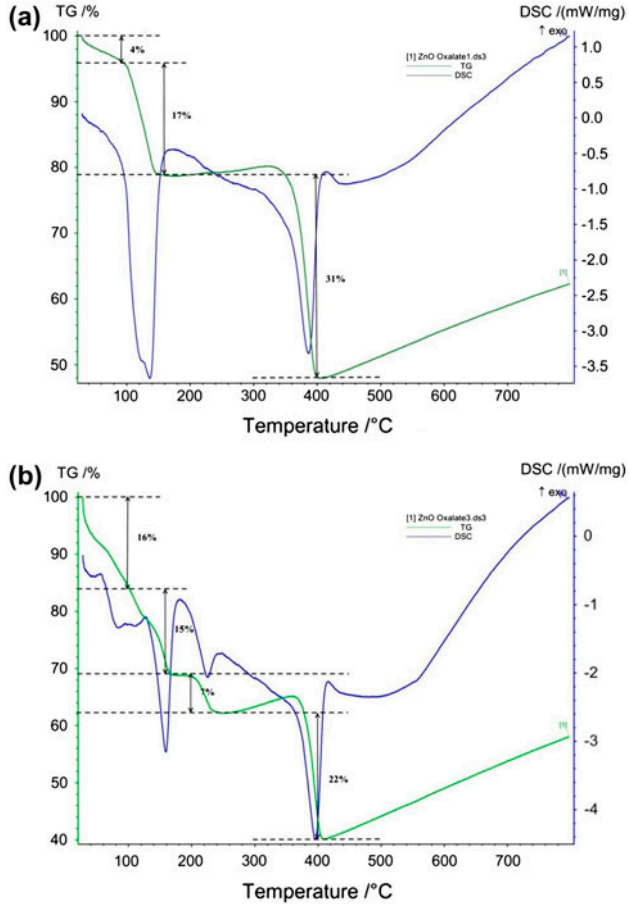

Fig. 1. TGA-DSC spectra: (a) Zinc oxalate without additives and (b) Zinc oxalate with EG.

$$Zn(CH_3COO)_2 \cdot 2H_2O + H_2C_2O_4 \cdot 2H_2O \overset{65^\circ C}{\rightarrow} ZnC_2O_4 \cdot 2H_2O + 2CH_3COOH + 2H_2O \quad (6)$$

$$CH_3COOH + C_2H_5OH \overset{65^\circ C}{\rightarrow} CH_3COOC_2H_5 + H_2O \quad (7)$$

$$ZnC_2O_4 \cdot 2H_2O \overset{below\,190^\circ C}{\rightarrow} ZnC_2O_4 + 2H_2O \quad (8)$$

$$ZnC_2O_4 \overset{360-400^\circ C}{\rightarrow} ZnO + CO + CO_2 \quad (9)$$

Fig. 1(a) demonstrated the heating profile of zinc oxalate dehydrate without any additives. It could be observed that there were two endothermic peaks according to the DSC curves and with obvious weight loss stages based on TGA curves. The first peak indicated the evaporation of ethanol and water, while the second peak showed the decomposition of zinc oxalate. For instance, the weight loss below 100˚C exhibited 4% of ethanol removal while the water removal occurred below 190˚C was approximately 17%. The significant weight loss of 31% at about 360–400˚C represented the complete conversion of zinc oxalate into pure zinc oxide. On the other hand, in Fig. 1(b), the heating profile of zinc oxalate with EG as additive displayed that there were more endothermic peaks when compared with Fig. 1(a). This could be explained that there was an additional stage of EG decomposition in between 100–200˚C [15] while other peaks were similarly as per reported in Fig. 1(a). The weight losses for several stages such as ethanol evaporation, EG removal, water removal, and decomposition of zinc oxalate were approximately 16, 15, 7, and 22%, respectively.

On both TGA-DSC curves, it was observed that the final calcination temperature for the complete reactions fell on 400˚C. It was a significant indicator, whereby no further reactions would occur beyond this temperature. The addition of EG as surfactant did not cause any significant effects on the calcination

temperature for the conversion of zinc oxalate to zinc oxide. Hence, the optimal calcination temperature for zinc oxalate precursors was at 400°C.

3.2. XRD analysis

The purity of synthesized ZnO NPs was investigated by performing XRD analysis. XRD analysis can be utilized to evaluate peak broadening with crystallite size and lattice strain. Crystallite size is performed by measuring the broadening of a particular XRD peak in a diffraction pattern associated with a particular planar reflection from within the crystal unit cell. The Bragg width contribution from crystallite size is inversely proportional to the crystallite size. Thus, the peak broadening indicates smaller crystallite size. Fig. 2 demonstrated the XRD pattern of the ZnO NPs where all the peaks indicate hexagonal wurtzite structure of ZnO (lattice parameters, $a = b = 3.249$ Å, $c = 5.206$ Å). Table 1 below showed the diffraction data agree well with the JCPDS card for ZnO (JCPDS 36-1451) with all (2θ) peaks at 31.73 (1 0 0), 34.35 (0 0 2), 36.24 (1 0 1), 47.53 (1 0 2), 56.60 (1 1 0), 62.80 (1 0 3), 67.90 (1 1 2), and 68.98 (2 0 1). From the data, it was observed that ZnO-EG show peaks broadening which signified smaller crystallite size when compared to ZnO with much higher and narrow peaks. Thus, the addition of EG in the synthesis of ZnO would help in the size reduction of ZnO NPs.

3.3. Fourier transform infrared spectroscopy

FTIR analysis was performed in Fig. 3 to study all the functional groups present between the zinc oxalate, zinc oxide, and zinc oxide functionalized with EG. The wave number at 3,300–3,500 cm^{-1} indicates the presence of O–H groups from water and ethanol. The strong C=O stretching peak around 1,600 cm^{-1} and the C–O moiety around 1,300 cm^{-1} were detectable. The presence of a peak at 820 cm^{-1} indicates that there is C–H groups coming from the precursors of ZnO synthesis. The most recognized peak of ZnO bond falls on wave number of 490–500 cm^{-1}. This was the last peak which illustrated the existence of final element after the calcination process. All the hydroxyl and carbonyl groups of zinc oxalate were completely removed after the calcination. The FTIR spectra for both ZnO with and without EG indicates that there is no significant effect on the presence of EG towards the purity of ZnO as there is not much difference between the curves.

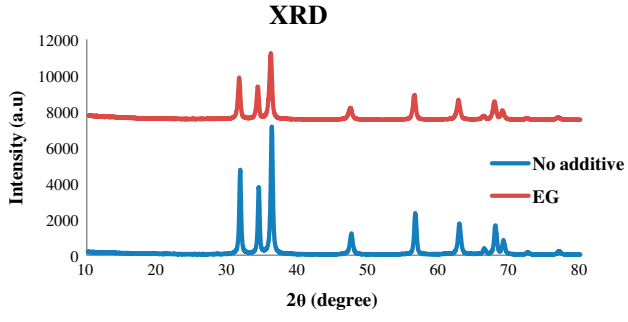

Fig. 2. XRD analysis for ZnO and ZnO-EG.

3.4. Surface morphology (FESEM & TEM) & dispersion property

The confirmation of NPs size and shape was verified by performing surface morphology analysis via FESEM and TEM. Fig. 4(a) and (b) showed the actual particles size of synthesized ZnO and ZnO with EG. It was observed that the size of ZnO NPs without any additives exhibited larger size with agglomerations, while the NPs with additives showed a better distribution of particles with smaller size and reduced agglomerations. The average particles size for ZnO without additives was around 50 ± 5 and 25 ± 5 nm for ZnO with surfactant. Fig. 4(c) and (d) demonstrated that all ZnO nanoparticle samples were spherically shaped. On the other hand, the dispersion property was checked using zetasizer. It was proven that the ZnO NPs in EG were well dispersed. Based on Fig. 5, The Z-average value of ZnO NPs is 282.2 d.nm while 28.09 d.nm for ZnO-EG. This shows that the ZnO-EG has better dispersion properties without agglomeration problem as the particles size is similar with TEM analysis in comparison with pure ZnO, which shows higher Z-average value. The higher the Z-average value indicated the agglomeration of smaller particles into bigger particles. Therefore, it signified that the particles were not distributed evenly.

3.5. Membrane application

3.5.1. Membrane performance

The performance of membrane was evaluated by performing water permeability analysis, rejection study, hydrophilicity study, and fouling study. In this case, the fabricated membranes embedded with different types of ZnO NPs were investigated and confirmed by applying several characterization methods. The basic performance findings for three different membranes [PSF, PSF-ZnO, and PSF-ZnO-EG] were summarized in Fig. 6. The enhancement of membrane

Table 1
Diffraction data of XRD

Peaks	1 0 0	0 0 2	1 0 1	1 0 2	1 1 0	1 0 3	1 1 2	2 0 1
ZnO	4,517	3,788	7,157	1,222	2,296	1,706	1,624	717
ZnO-EG	1,822	1,492	2,475	522	1,000	987	921	552

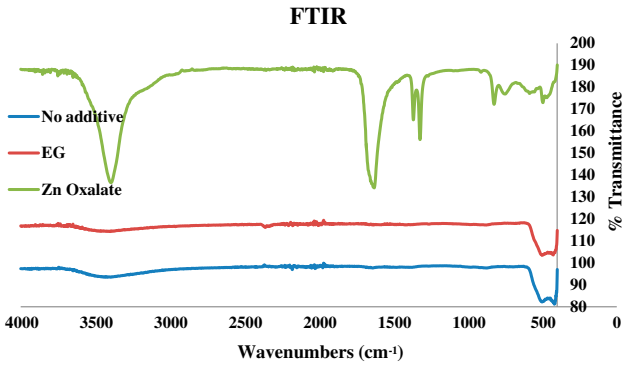

Fig. 3. FTIR analysis for zinc oxalate, ZnO, and ZnO-EG.

application was attributed to the unique properties of ZnO NPs, which were uniformly dispersed in the structure of PSF membranes.

The surface wettability study of the membranes was equally important as an indicator of hydrophilicity. Contact angle study was a measurement for membrane wettability. The high value of contact angle indicated higher hydrophobicity and vice versa. The pure PSF exhibited highest contact angle of 69.7˚ and the addition of ZnO and ZnO-EG had reduced the contact angle to 53.3 and 43.1, respectively. The main reason was ZnO NPs had higher affinity toward water, which resulted in better surface hydrophilicity [16]. Besides, the presence of EG as naturally hydrophilic surfactant onto the ZnO NPs greatly enhanced the hydrophilicity of the membranes. This was mainly due to EG molecule establishing a strong affinity with water molecules and the OH structure in EG would form a hybrid with water molecules [17]. The incorporation of ZnO NPs has enhanced the hydrophilicity of membranes as reported in several previous studies [9,18].

In addition, hydrophilicity of membranes indicated direct correlation on water permeability. Fig. 6(i) and (ii) showed that the water permeability had increased proportionately with the hydrophilicity of the membranes when the membranes were incorporated with ZnO-EG NPs. The water permeability rate improved due to the enhancement in the interaction between the hydrophilic ZnO-EG membrane and water molecules [19]. Therefore, the naturally hydrophilic PSF-ZnO-EG composite membranes exhibited highest permeability when compared to the pure PSF and PSF-ZnO membranes. Besides, the size of ZnO-EG NPs were smaller than ZnO NPs, which resulted in higher reacting surface area in membrane structure and well dispersed due to the reduced conglomerations problem. Thus, it resulted in the reduction of the hydraulic resistance of water.

The mass transfer between the solvent and nonsolvent phase was delayed during phase inversion process with highly viscous casting solution, which led to low porosity membranes [20]. According to this result, the membranes with high porosity and smaller pore size were produced in the presence of hydrophilic ZnO-EG NPs. This was mainly due to the improved hydrophilicity of PSF-ZnO-EG casting solution, which assisted in the mass transfer during the phase inversion process. Thus, it would form more porous membrane structure. Moreover, the increment in pore size could be attributed to the acceleration of exchange rate between solvent and nonsolvent during phase inversion [21]. The pore size could also be affected by the nucleation process of ZnO as the heterogeneous nucleation of ZnO would increase the crystallinity of the NPs [22]. The pore size findings were further confirmed by the porosity data, which resulted in higher porosity for membrane incorporated with ZnO and ZnO-EG NPs.

Rejection study was performed by applying humic acid solution. From the result, the rejection percentage increase from 70 to 86% for membrane with ZnO and ZnO-EG, while 88% for pure PSF. There was a decrement of rejection percentage when the membrane was incorporated with normal ZnO NPs without any additives while a good improvement when the membranes were embedded with functionalized ZnO NPs. This was mainly due to the functionalized ZnO with EG had better antifouling properties, which would reduce the adsorption of organic pollutants within membrane structure [8]. Thus, it contributed to the retention of organic matter during the filtration process. The improved hydrophilicity of the ZnO NPs would enhance the fouling resistance of the membranes. By establishing highly hydrophilic membrane structure, the hydraulic resistance of membrane could be reduced. This was probably due to higher affinity

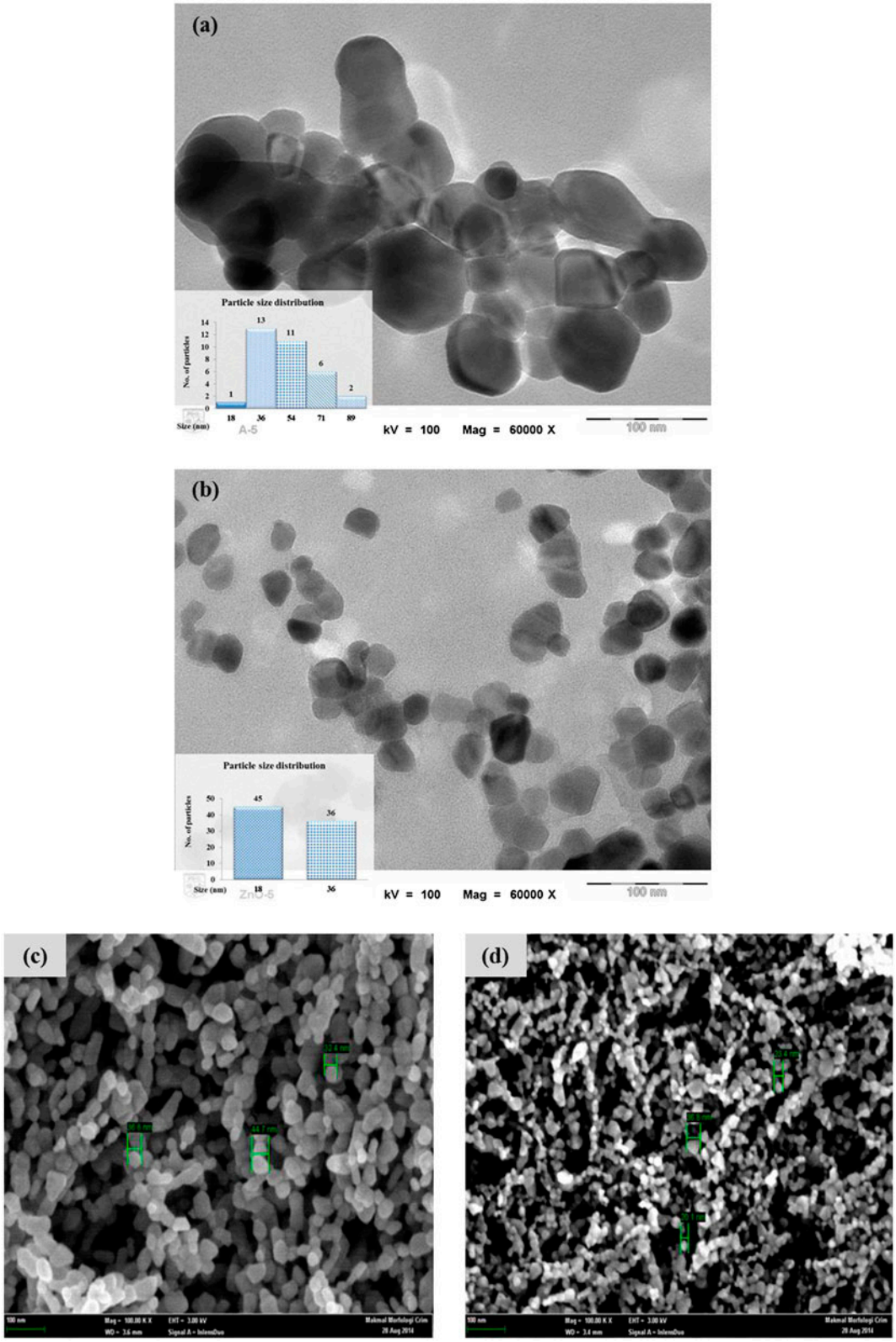

Fig. 4. ZnO Morphology: TEM images: (a) without additive, (b) with EG; FESEM images: (c) without additive, and (d) with EG.

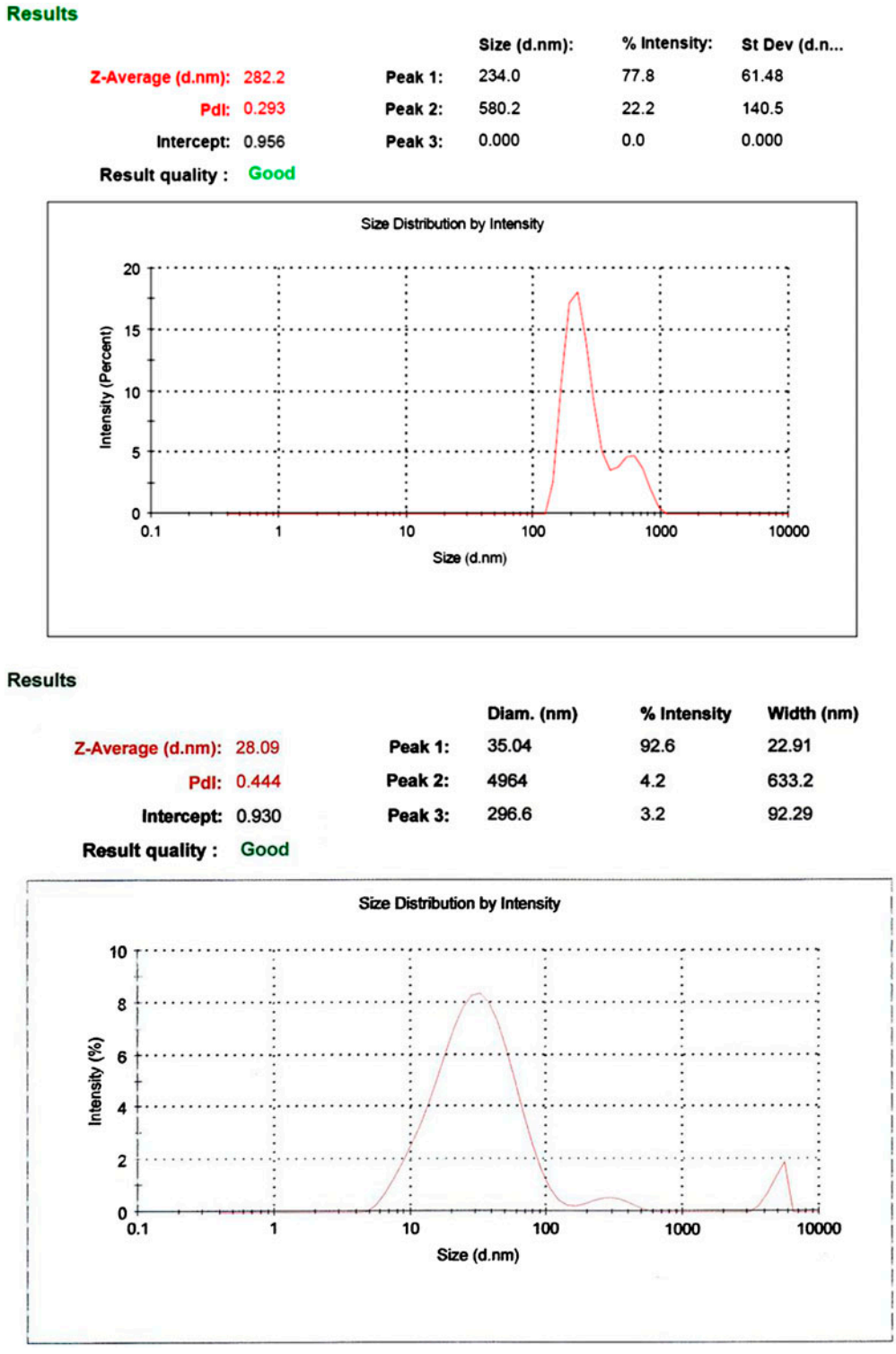

Fig. 5. Zetasizer analysis: (i) ZnO and (ii) ZnO-EG.

of ZnO towards water, which reduced the hydrophobic adsorption between humic acid molecules and ZnO-incorporated membranes [23].

The structure for the three types of membrane is shown from the SEM images in Fig. 7. There was no significant impact on the structure alterations

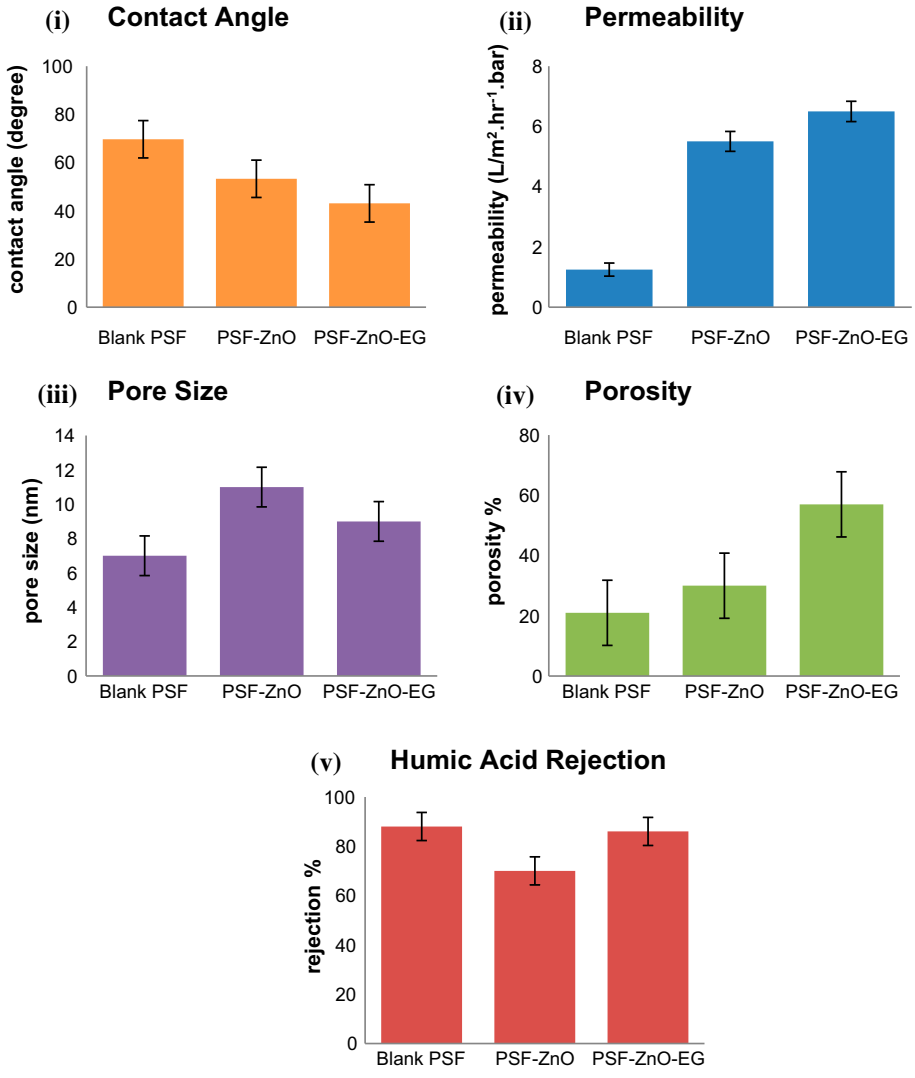

Fig. 6. Membrane performance for Blank PSF, PSF-ZnO, PSF-ZnO-EG: (i) Contact angle, (ii) Permeability, (iii) Pore size, (iv) Porosity, and (v) Humic acid rejection.

when the ZnO NPs were embedded in the membrane. This indicated that the addition of ZnO NPs did not affect the membrane cross sections. It was observed that only a slight change in the pore size which was similar to the pore size findings. All the membrane structure exhibited a typical asymmetric morphology with fingerlike pores linked by sponge walls [24]. Therefore, it could be assumed that no alterations occurred during the formation mechanism of PSF membrane with ZnO and functionalized ZnO NPs.

From all the aspects mentioned above, the membranes fabrication with embedded ZnO NPs is highly favorable for various kinds of filtration due to its essential properties in terms of permeability, rejection capability, and porosity. The improvement of membrane performance was contributed by improved hydrophilicity of ZnO and ZnO-EG NPs. The hydrophilic nature of the PSF-ZnO-EG also enhanced the water permeation rate, wettability of membrane surface, and also improved fouling resistance toward organic matter. The reduction size of functionalized ZnO NPs had higher reacting surface area and well dispersion in the structure [25]. The ZnO-EG NPs decreased agglomerations problem and caused less pores blockage in membrane structure. Hence, the performance of membrane could be highly improved.

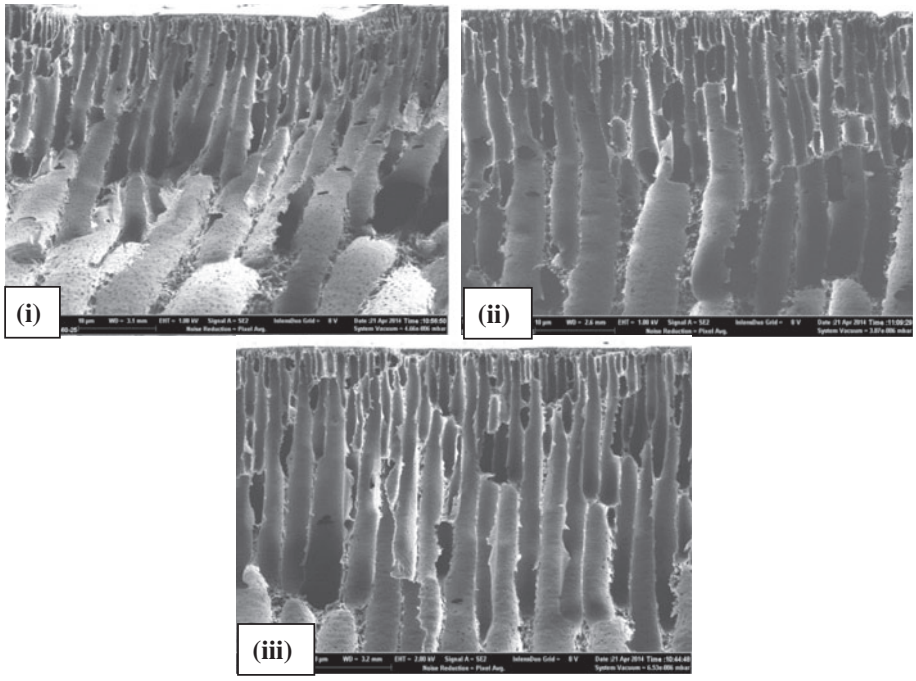

Fig. 7. SEM images: (i) Blank PSF, (ii) PSF-ZnO, and (iii) PSF-ZnO-EG.

4. Conclusion

ZnO NPs are alternative nanomaterials which possess unique characteristics for various types of industrial applications. The enhancement of NPs performance was investigated by functionalization with additives. The impact of EG as an additive in the ZnO synthesis via sol–gel method was compared with the normal synthesis of ZnO. From the data analysis, XRD patterns indicated the wurtzite structure and the hexagonal phase of ZnO NPs for both with and without additive synthesis. It was observed that the particles produced by addition of EG were in spherical shape with reduced agglomeration. The average particles size was reduced from the range of 50–60 nm (without additives) to 20–30 nm (with EG). ZnO-EG had better dispersion properties, which was proven by zetasizer analysis as the Z-average value of ZnO NPs was 282.2 d nm while 28.09 d nm for ZnO-EG which was similar to TEM. The synthesized NPs were then incorporated in the PSF membrane fabrication. The novelty of the functionalized ZnO NPs with EG was the significant improvement of its well-dispersed properties and great hydrophilicity, which further enhanced the membrane development process. The reduced size of ZnO NPs with less agglomerations problems was highly favorable in various membrane applications. PSF-ZnO-EG membrane showed better membrane performances than that of PSF and ZnO membranes because its hydrophilic nature had contributed to the enhancement of membrane performance in terms of permeability, porosity, rejection ability, and hydrophilicity.

Acknowledgment

The authors would like to gratefully acknowledge NPRP grant #[5-1425-2-607] from the Qatar National Research Fund (a member of Qatar Foundation) for the financial support in this study. Besides, the authors wish to acknowledge the Ministry of Education Malaysia for sponsoring Ying Tao Chung postgraduate study via MyBrain and CRIM (Centre for Research and Instrumentation Management, UKM) for XRD, FESEM, and TEM analyses.

References

[1] V. Srivastava, D. Gusain, Y.C. Sharma, Synthesis, characterization and application of zinc oxide nanoparticles (n-ZnO), Ceram. Int. 39 (2013) 9803–9808.
[2] L.Y. Ng, A.W. Mohammad, C.P. Leo, N. Hilal, Polymeric membranes incorporated with metal/metal oxide nanoparticles: A comprehensive review, Desalination 308 (2013) 15–33.
[3] D.Y. Koseoglu-Imer, B. Kose, M. Altinbas, I. Koyuncu, The production of polysulfone (PS) membrane with silver nanoparticles (AgNP): Physical properties, filtration performances, and biofouling resistances of membranes, J. Membr. Sci. 428 (2013) 620–628.

[4] M.M. Ba-Abbad, A.A.H. Kadhum, A.B. Mohamad, M.S. Takriff, Synthesis and catalytic activity of TiO_2 nanoparticles for photochemical oxidation of concentrated chlorophenols under direct solar radiation, Int. J. Electrochem. Sci. 7 (2012) 4871–4888.
[5] J. Yin, E.-S. Kim, J. Yang, B. Deng, Fabrication of a novel thin-film nanocomposite (TFN) membrane containing MCM-41 silica nanoparticles (NPs) for water purification, J. Membr. Sci. 423–424 (2012) 238–246.
[6] I. Sawada, R. Fachrul, T. Ito, Y. Ohmukai, T. Maruyama, H. Matsuyama, Development of a hydrophilic polymer membrane containing silver nanoparticles with both organic antifouling and antibacterial properties, J. Membr. Sci. 387–388 (2012) 1–6.
[7] J.-H. Li, Y.-Y. Xu, L.-P. Zhu, J.-H. Wang, C.-H. Du, Fabrication and characterization of a novel TiO_2 nanoparticle self-assembly membrane with improved fouling resistance, J. Membr. Sci. 326 (2009) 659–666.
[8] S. Balta, A. Sotto, P. Luis, L. Benea, B. Van der Bruggen, J. Kim, A new outlook on membrane enhancement with nanoparticles: The alternative of ZnO, J. Membr. Sci. 389 (2012) 155–161.
[9] C.P. Leo, W.P. Cathie Lee, A.L. Ahmad, A.W. Mohammad, Polysulfone membranes blended with ZnO nanoparticles for reducing fouling by oleic acid, Sep. Purif. Technol. 89 (2012) 51–56.
[10] M.M. Ba-Abbad, A.A.H. Kadhum, A. Bakar Mohamad, M.S. Takriff, K. Sopian, The effect of process parameters on the size of ZnO nanoparticles synthesized via the sol–gel technique, J. Alloys Compd. 550 (2013) 63–70.
[11] M.M. Ba-Abbad, A.A.H. Kadhum, A.B. Mohamad, M.S. Takriff, K. Sopian, Visible light photocatalytic activity of Fe^{3+}-doped ZnO nanoparticle prepared via sol–gel technique, Chemosphere 91 (2013) 1604–1611.
[12] K.G. Kanade, B.B. Kale, R.C. Aiyer, B.K. Das, Effect of solvents on the synthesis of nano-size zinc oxide and its properties, Mater. Res. Bull. 41 (2006) 590–600.
[13] G. Nabiyouni, A. Barati, M. Saadat, Surface adsorption of polyethylene glycol and polyvinyl alcohol with variable molecular weights on zinc oxide nanoparticles, Iran. J. Chem. Eng. 8 (2011) 20–30.
[14] M.A. Behnajady, N. Modirshahla, E. Ghazalian, Synthesis of ZnO nanoparticles at different conditions: A comparison of photocatalytic activity, Digest J. Nanomater. Biostructures 6 (2011) 467–474.
[15] Y. Tseng, M. Chuang, Y. Chen, C. Wu, Synthesis of 1D, 2D, and 3D ZnO polycrystalline nanostructures using the sol–gel method, J. Nanotechnol. 2012 (2012) 1–8, doi: 10.1155/2012/712850.
[16] J. Hong, Y. He, Effects of nano sized zinc oxide on the performance of PVDF microfiltration membranes, Desalination 302 (2012) 71–79.
[17] X. Zhang, Y. Wang, Y. Liu, J. Xu, Y. Han, X. Xu, Preparation, performances of PVDF/ZnO hybrid membranes and their applications in the removal of copper ions, Appl. Surf. Sci. 316 (2014) 333–340.
[18] F. Shi, Y. Ma, J. Ma, P. Wang, W. Sun, Preparation and characterization of PVDF/TiO_2 hybrid membranes with different dosage of nano-TiO_2, J. Membr. Sci. 389 (2012) 522–531.
[19] M.J. Kao, D.C. Tien, C.S. Jwo, T.T. Tsung, The study of hydrophilic characteristics of ethylene glycol, J. Phys. Conf. Ser. 13 (2005) 442–445.
[20] H. Wu, B. Tang, P. Wu, Development of novel SiO_2–GO nanohybrid/polysulfone membrane with enhanced performance, J. Membr. Sci. 451 (2014) 94–102.
[21] H. Wu, B. Tang, P. Wu, Novel ultrafiltration membranes prepared from a multi-walled carbon nanotubes/polymer composite, J. Membr. Sci. 362 (2010) 374–383.
[22] S. Qiu, L. Wu, X. Pan, L. Zhang, H. Chen, C. Gao, Preparation and properties of functionalized carbon nanotube/PSF blend ultrafiltration membranes, J. Membr. Sci. 342 (2009) 165–172.
[23] Y.H. Teow, A.L. Ahmad, J.K. Lim, B.S. Ooi, Studies on the surface properties of mixed-matrix membrane and its antifouling properties for humic acid removal, J. Appl. Polym. Sci. 128 (2013) 3184–3192.
[24] E. Mahmoudi, L.Y. Ng, M.M. Ba-Abbad, A.W. Mohammad, Novel nanohybrid polysulfone membrane embedded with silver nanoparticles on graphene oxide nanoplates, Chem. Eng. J. 277 (2015) 1–10.
[25] L. Shen, X. Bian, X. Lu, L. Shi, Z. Liu, L. Chen, Z. Hou, K. Fan, Preparation and characterization of ZnO/polyethersulfone (PES) hybrid membranes, Desalination 293 (2012) 21–29.